Author Manuscript

Author Manuscript

Author Manuscript

Author Manuscript

HHS Public Access

Author manuscript

Cell Rep. Author manuscript; available in PMC 2022 April 21.

Published in final edited form as:

Cell Rep. 2020 January 14; 30(2): 454–464.e5. doi:10.1016/j.celrep.2019.12.048.

Large 1p36 Deletions Affecting *Arid1a* Locus Facilitate *Mycn*-Driven Oncogenesis in Neuroblastoma

Jesus García-López[1,*], **Kirby Wallace**[2,7,8], **Joel H. Otero**[3,8], **Rachelle Olsen**[4,8], **Yong-dong Wang**[5], **David Finkelstein**[5], **Brian L. Gudenas**[1], **Jerold E. Rehg**[6], **Paul Northcott**[1], **Andrew M. Davidoff**[2], **Kevin W. Freeman**[7,9,*]

[1]Department of Developmental Neurobiology, St. Jude Children's Research Hospital, Memphis, TN, USA

[2]Department of Surgery, St. Jude Children's Research Hospital, Memphis, TN 38105, USA

[3]Department of Hematology, St. Jude Children's Research Hospital, Memphis, TN 38105, USA

[4]Department of Oncological Sciences, Huntsman Cancer Institute, Salt Lake City, UT 84112, USA

[5]Computational Biology Department, St. Jude Children's Research Hospital, Memphis, TN 38105, USA

[6]Pathology Department, St. Jude Children's Research Hospital, Memphis, TN 38105, USA

[7]Genetics, Genomics & Informatics, The University of Tennessee Health Science Center (UTHSC), Memphis, TN 38103, USA

[8]These authors contributed equally

[9]Lead Contact

SUMMARY

Loss of heterozygosity (LOH) at 1p36 occurs in multiple cancers, including neuroblastoma (NBL). *MYCN* amplification and 1p36 deletions tightly correlate with markers of tumor aggressiveness in NBL. Although distal 1p36 losses associate with single-copy *MYCN* tumors, larger deletions correlate with *MYCN* amplification, indicating two tumor suppressor regions in 1p36, only one of which facilitates *MYCN* oncogenesis. To better define this region, we genome-edited the syntenic 1p36 locus in primary mouse neural crest cells (NCCs), a putative NBL cell of origin. In *in vitro* cell transformation assays, we show that *Chd5* loss confers most of the *MYCN*-independent tumor suppressor effects of 1p36 LOH. In contrast, *MYCN*-driven tumorigenesis selects for NCCs with *Arid1a* deletions from a pool of NCCs with randomly sized

This is an open access article under the CC BY-NC-ND license (http://creativecommons.org/licenses/by-nc-nd/4.0/).

[*]Correspondence: jesus.garcialopez@stjude.org (J.G.-L.), kfreem22@uthsc.edu (K.W.F.).

AUTHOR CONTRIBUTIONS

J.G.-L., K.W.F., Y.W., B.L.G., and D.F. analyzed the data. J.G.-L. and K.W.F. conceived methods for analyzing data. J.G.-L. performed experiments. J.G.-L., K.W.F., J.H.O., and R.O. collected samples and information. J.G.-L. and K.W.F. designed the study. J.G.-L. and K.W.F. wrote the manuscript with input from K.W.F., Y.W, D.F., A.M.D., P.N., R.O., and J.E.R.

SUPPLEMENTAL INFORMATION

Supplemental Information can be found online at https://doi.org/10.1016/j.celrep.2019.12.048.

DECLARATION OF INTERESTS

The authors declare no competing interests.

Author Manuscript Author Manuscript Author Manuscript Author Manuscript

1p36 deletions, establishing *Arid1a* as the *MYCN*-associated tumor suppressor. Our findings reveal that *Arid1a* loss collaborates with oncogenic *MYCN* and better define the tumor suppressor functions of 1p36 LOH in NBL.

Graphical Abstract

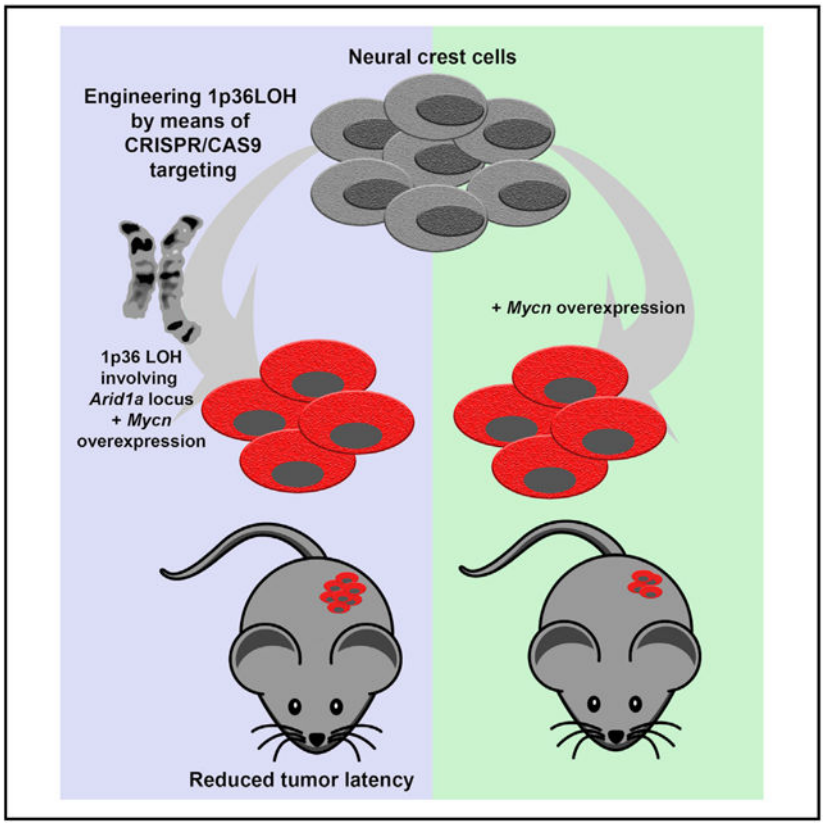

In Brief

Garcia-Lopez et al. present a mouse model of high-risk neuroblastoma that includes 1p36 loss and *Mycn* overexpression. This study substantiates previous predictions from NBL genetic studies, which proposed that two tumor suppressor regions exist in 1p36. It further demonstrates that *Mycn* overexpression selects for loss of *Arid1a* during tumorigenesis.

INTRODUCTION

Chromosomal instability (CIN) is found in 90% of cancers, and worse instability associates with poorer prognosis (Hanahan and Weinberg, 2011; Pikor et al., 2013). CIN leads to whole or segmental gains and losses of chromosomes, which are postulated to initiate cancer because these chromosomal abnormalities are detectable in premalignant lesions (Pikor et al., 2013). Though commonly associated with cancer, the contribution of these chromosomal alterations to malignant transformation is poorly understood. Deletion of 1p36 is a frequent segmental chromosomal loss found in different human cancers, including those of neural, epithelial, and hematopoietic origin (Godfried et al., 2002; Poetsch et al., 2003).

Author Manuscript Author Manuscript Author Manuscript Author Manuscript

The simultaneous loss of multiple gene-dosage sensitive tumor suppressors is the un-tested hypothesis for how 1p36 loss contributes to oncogenesis (Bagchi and Mills, 2008; Chen et al., 2018; Henrich et al., 2012).

Although a broad range of human cancers present 1p36 deletion, it is particularly frequent in a subset of cancers that affect the nervous system (Barbashina et al., 2005; Nakane et al., 2007; Tews et al., 2006) including high-risk neuroblastoma (NBL) (Carén et al., 2007; White et al., 2001). Few recurrent somatic mutations beyond segmental chromosomal gains and losses are found in NBL (Pugh et al., 2013), indicating that these segmental changes might initiate NBL. This makes NBL ideal for studying the contribution of these chromosomal alterations to oncogenesis. The genetics of 1p36 deletion has been extensively studied in NBL (Brodeur, 2003), with ~70% of *MYCN*-amplified NBL associated with 1p36 deletions (Huang and Weiss, 2013; Maris et al., 2001; Scaruffi et al., 2004). This indicates cooperation between a tumor suppressor that resides in 1p36 and *MYCN*-driven oncogenesis. Deletion mapping studies identified shorter deletions that map from 1p36.2 to 1p36.3 in *MYCN* single-copy NBL, while *MYCN*-amplified NBLs have larger deletions extending from 1p35 to at least 1p36.1 (Cheng et al., 1995; Spieker et al., 2001). These findings predict two distinct 1p36 tumor suppressor regions: a distal tumor suppressor region that associates with both *MYCN* single-copy and *MYCN*-amplified NBL and a proximal tumor suppressor region that associates with *MYCN*-amplified NBL.

Although a series of studies have implicated *CHD5* as a likely critical distal tumor suppressor in NBL, no studies have identified the proximal tumor suppressor. However, *ARID1A* has emerged as a tumor suppressor gene on the proximal 1p36.1 locus, which is mutated in a broad spectrum of cancers (Cho et al., 2015; Jiang et al., 2015; Wei et al., 2014). In particular, *ARID1A* is the only gene in the 1p36 locus presenting point mutations in NBL patients (Sausen et al., 2013), and it is located in the proposed proximal 1p36 tumor suppressor region, making it a promising proximal 1p36 tumor suppressor candidate. Relatedly, pan-cancer studies of somatic copy number alterations (SCNAs) in 3,131 cancers from 26 cancer types and 4,934 cancers from 11 cancer types found significant recurrent focal SCNAs in 140 and 158 regions, respectively, with shared regions of deletion across cancers at 1p36.31, the *CHD5* locus, and at 1p36.11, the *ARID1A* locus implicating the loss of these two loci in a number of cancers (Beroukhim et al., 2010; Zack et al., 2013). Whether 1p36 loss contributes to cancer development and which tumor suppressor genes from this region are involved in tumorigenesis are still unanswered questions in cancer (Carén et al., 2007; Henrich et al., 2012; Poetsch et al., 2003).

NBL arises from the developing sympathoadrenal lineage of the neural crest, and it is the most frequently diagnosed solid tumor malignancy in the first year of life (Cheung and Dyer, 2013). Neural crest cells (NCCs) migrate throughout the body and differentiate into many different cell types, including peripheral neurons and Schwann cells (Huang and Saint-Jeannet, 2004). The impairment of NCC development is postulated to be causative in NBL disease, and a histology-grading system has been established on the basis of the degree of differentiation, the Schwannian stromal content, and mitotic-karyorrhexis index (Shimada et al., 1999). Previously, we established a mouse model of NBL by the enforced expression of *Mycn* in primary mouse NCCs (Olsen et al., 2017). The resulting tumors

Author Manuscript Author Manuscript Author Manuscript Author Manuscript

recapitulate many of the salient aspects of human NBL, including deletions in a subset of tumors at the mouse syntenic 1p36 locus, indicating the utility of this approach to decipher the contributions of 1p36 deletion to NBL tumorigenesis and its cooperation with *Mycn*.

In this study, we used genome-editing technology, transformation of primary NCCs, and deep sequencing to deconvolute the contribution of 1p36 deletions to cancer initiation. Our data indicate that loss of the distal tumor suppressor *Chd5* or deletion of 1p36 confers pro-oncogenic traits in NCCs when *Mycn* is expressed at endogenous levels. In contrast, *Mycn* overexpression significantly selects for loss of *Arid1a* during tumor development, thus providing a rationale for why larger 1p36 deletions associate with *Mycn* amplification in NBL. These findings help decipher the various contributions of 1p36 deletions to NBL and lay the foundation for understanding the tumor suppressor functions of this locus in a broad spectrum of cancers.

RESULTS

Engineering Human 1p36 Deletions in Mouse Neural Crest Cells

To confirm, as previously reported, whether two different tumor suppressor regions in 1p36 locus are present in NBL tumors, we interrogated next-generation sequencing from the TARGET database. We verified the strong association between *MYCN* amplification and 1p36 deletion, with 79% of *MYCN*-amplified tumors (52 of 66) having 1p36 deletions (Figure 1A). Further analysis to determine the smallest region of overlap (SRO) (Caron et al., 2001; Mosse et al., 2005) defined a distal tumor suppressor loci including 1p36.23–32 for non-amplified *MYCN* tumors and a proximal region extending from 1p36.1 to 1p35.3 locus (Figure 1A). *CHD5* is located in the distal 1p36 region and has been characterized as a NBL tumor suppressor by multiple groups (Bagchi et al., 2007; Fujita et al., 2008). In contrast, the proximal region remains poorly characterized. *ARID1A* and *RUNX3* genes have been suggested as potential candidates, but only *ARID1A* has been shown to be mutated in NBL (Sausen et al., 2013; Yu et al., 2014). This led us to selectively target the two prominent tumor suppressor candidates for the distal and proximal regions of 1p36, *Chd5* and *Arid1a*, and to recapitulate the human 1p36 deletion. This was done in primary NCCs isolated from day 9.5 mouse embryos, which enables direct comparison of *Arid1a* and *Chd5* deletions with loss of the entire 1p36 locus in a genetically normal background. The deleted genomic region encompasses *Arid1a* and *Chd5* and an intervening 20 Mb with 238 coding genes. First, to determine the efficiency of our system, we validated the guide RNAs (gRNAs) individually and also as part of an all-in-one vector. Western blot (WB) analysis confirmed that Arid1a and Chd5 protein levels decreased after the introduction of gRNAs (Figure 1B). Then, we addressed the existence of large chromosomal losses by fluorescence *in situ* hybridization (FISH) (Figure 1C) and karyotype analysis (Figure 1D). Both karyotype and FISH analysis only reported cells that lost the 1p36 locus in one allele, suggesting either a lethality of homozygous deletion or a growth advantage for cells that maintain at least one of their chromosomal copies.

Author Manuscript Author Manuscript Author Manuscript Author Manuscript

Loss of the 1p36-Syntenic Region and Depletion of *Chd5* in NCCs Induce Colony Formation and Markedly Impair Migration, whereas *Arid1a* Collaborates with *Mycn* Overexpression

We first modeled the MYCN-independent roles of the 1p36 locus. To evaluate the tumorigenic potential of NCCs depleted of *Arid1a*, *Chd5*, or the 1p36-syntenic region, we performed colony formation assays *in vitro*. Three different NCC lines were engineered and compared with wild-type NCCs (WT NCCs) in this assay to assess if cells with 1p36 syntenic deletions and cells with *Arid1a* or *Chd5* deletions had growth advantage in soft agar cultures. Whereas the vast majority of WT NCCs (≈90%) became senescent, the NCCs lacking 1p36-syntenic region, *Arid1a*, or *Chd5* had increased colony-forming capabilities (Figure 2A). The greatest extent of colony growth was seen for *Chd5*-depleted NCCs, with about 85% growing as colonies (Figure 2A). The anchorage-independent growth capabilities were greater in cells depleted of *Chd5* in comparison with those lacking the 1p36-syntenic region. We also tested the transforming capabilities of *Mycn* overexpression alone or in combination with either 1p36-syntenic region, *Arid1a*, or *Chd5* loss (Figure S1). Nearly 100% of NCCs transformed with *Mycn* overexpression grow as colonies, confirming the potent oncogenic capabilities of this gene. NCCs with loss of *Arid1a* tolerated *Mycn*-driven colony formation, while NCCs with loss of *Chd5* or loss of the syntenic 1p36 region interfered significantly with *Mycn* colony-forming capabilities, suggesting, in this particular assay, a preference for retaining *Chd5*.

Next, we tested the migration capabilities of genetically modified NCCs in a wound healing assay. The healing and cell migration rates were significantly increased ($p < 0.05$) in cells depleted of 1p36-syntenic locus or *Chd5*. In contrast, no differences were observed in cells depleted of *Arid1a* expression in comparison with WT NCCs (Figure 2B). The results showed that the downregulation of *Chd5* is pro-oncogenic for NCCs in *in vitro* assays of transformation. As loss of the whole 1p36-syntenic region did not show any growth or migratory advantage compared with NCCs with reduced *Chd5* expression, we next evaluated cell proliferation and differentiation capabilities.

NCCs Depleted of *Arid1a, Chd5*, or 1p36 LOH Showed Normal Proliferative Rates but Impairment in Differentiation

The impairment of cell differentiation and the deregulation of proliferative capabilities are two important hallmarks of cell transformation. To assess the role of *Arid1a*, *Chd5*, and 1p36 loss during NCC development, we carried out proliferation and differentiation studies under different media conditions.

Proliferation rates were assessed for NCCs that were expanded undifferentiated in chemically defined media (CDM), but no differences were observed among the different NCC populations evaluated (Figure 2C), suggesting that the depletion of *Arid1a*, *Chd5*, or 1p36 region is not promoting any proliferation advantage under such culture conditions. In contrast, when cells were cultured on CDM depleted of growth factors to promote neuronal differentiation and then analyzed using Ki67 staining, NCCs lacking 1p36-syntenic region showed increased proliferative rates (Figure 2D). This result strongly suggested the existence of a subpopulation of uncommitted NCCs cells that did not respond properly

Author Manuscript Author Manuscript Author Manuscript Author Manuscript

to differentiation signals, maintaining their proliferative capabilities. To confirm impaired differentiation, NCCs were cultured in neuronal differentiation conditions for 8 days and then analyzed for expression of common neuronal differentiation markers (Figures 3A and 3B). As NCCs differentiate into dopaminergic neurons, they lose expression of ASCL1 while increasing the expression of PHOX2B, tyrosine hydroxylase (TH), and the neuron-specific cytoskeletal proteins TUJ1 and MAP2, which are involved in determining and stabilizing dendritic shape during neuron development. Whereas WT NCCs were able to create neurons and neuronal networks, cells lacking *Arid1a*, *Chd5*, or the 1p36-syntenic region showed neuronal differentiation deficiencies (Figure 3B). The most undifferentiated were cells depleted of *Chd5* and the cells that lost the 1p36-syntenic region. The data show a significant reduction of expression for TUJ1 and MAP2 in Chd5 and 1p36-depleted cells and complete loss of TH expression. ARID1A-depleted cells showed a modest reduction in expression of all three markers (Figure 3B). We additionally checked whether neurons were still maintaining Arid1a and Chd5 expression after 7 days on neurogenic medium (Figure S2). The analysis confirmed that cells depleted of 1p36-syntenic region or CHD5 presented severe deficiencies in neurogenesis. Moreover, cells lacking the whole syntenic region maintain proliferative capabilities, suggesting an additional tumor suppressor loss that helps support proliferation. More modestly, the downregulation of *Arid1a* displayed a less severe effect on differentiation, but neurite formation was reduced considerably, and the expression of neuronal markers showed differences from WT NCCs. An impairment of normal differentiation is postulated to contribute to NBL oncogenesis, and we observe, to varying degrees, that loss of 1p36, *Chd5*, and *Arid1a* impair differentiation of the NBL stem population (the NCCs).

Modeling High-Risk NBL *In Vivo* through NCC Transformation

Because MYCN is sufficient to achieve nearly 100% colony formation in the *in vitro* soft agar assay, we were prevented from assessing the contribution of Chd5, Arid1a, or entire 1p36 region loss in MYCN-driven tumorigenesis in this assay. To assess this we instead used a more rigorous *in vivo* tumor-forming assay. To model NBL *in vivo* and determine the *MYCN*-associated 1p36 tumor suppressor, we engineered three different NCC lines by genome-editing them to have randomly sized 1p36 deletions. These deletions are at the two loci, *Arid1a* and *Chd5*, up to large deletions that include loss of the entire syntenic 1p36 region. To accomplish this, independent transfections using an all-in-one vector containing several gRNAs targeting *Arid1a* and *Chd5* locus were performed. Because the non-homologous end-joining (NHEJ) repair system can generate large chromosomal losses from single insertions or deletions (indels), we predicted that introducing a heterogeneous population of cells containing depletion of *Arid1a* and *Chd5* loci or containing whole 1p36 loss could allow us to address which genetic and genomic aberrations are positively selected for during *Mycn*-driven tumorigenesis. Our *in vitro* approach found that by combining two sets of gRNAs targeting *Arid1a* and *Chd5* simultaneously in the same construction, we could generate chromosomal losses mimicking 1p36 loss of heterozygosity (LOH) in a range varying from 2.5% to 85% of cells as assessed using FISH and karyotyping (from now on we refer to these cells as 1p36-del and the tumors generated using them in combination with Mycn as 1p36-del/Mycn). Finally, WT NCCs in combination with or without *Mycn* overexpression were also injected. All of the mice injected with *Mycn* NCCs (n = 10)

Author Manuscript Author Manuscript Author Manuscript Author Manuscript

developed tumors with a broad range of 61–124 days (Figure 4A); just one of ten animals presented tumors earlier than 90 days. This demonstrates, as we previously reported, that *Mycn* overexpression is sufficient to generate NBL in mice (Olsen et al., 2017). The 1p36-del NCCs (n = 17) and WT NCCs (n = 10) did not generate any tumor by themselves 12 months after injection. However, seven of eight animals injected with 1p36-del/Mycn NCCs developed tumors, and just one these tumors was detected after 85 days post-injection. The crossing survival curve indicates non-proportional hazards with two hazard functions involved. For the first hazard function, latency, we calculated log rank (Mantel-Cox) with 1p36-del/Mycn NCCs showing an acceleration of tumor onset ($p < 0.001$) compared with tumors from *Mycn* NCCs (Figure 4A). The second hazard, tumor penetrance, was not significantly different. Overall, the loss of a tumor suppressor in the 1p36-syntenic region reduces the time frame for *Mycn*-driven tumorigenesis.

Tumors were isolated before they reached 2 cm^3, and the histopathological analysis revealed that all were neuroectodermal tumors with morphologic features similar to the transgenic *Th-NMyc* NBL mouse (Teitz et al., 2011). All tumors were composed of a highly proliferative population of cells resulting in a high mitotic index (5/hpf). Tumors generated by NCCs overexpressing MYCN showed strong GFAP immunoreactivity, indicating Schwannian stroma, and 95% of the tumor cells were MAP2 negative or very weakly positive (Figure 4B). In contrast, 1p36-del/*Mycn* tumors had regions with strong immune reactivity for GFAP, but in general most of the cells were negative or weakly positive for GFAP. These tumors also had moderate to strong cytoplasmic MAP2 immunoreactivity (Figure 4B). The synaptophysin staining highlighted other differences between the tumors obtained from different genetically modified cell combinations. Tumors that developed from *Mycn* NCCs were mostly negative for synaptophysin, having some areas of weak immunoreactivity (corresponding to 5% of tumor cell population), whereas tumors from 1p36-del/*Mycn* NCCs had multiple small foci of cells with moderate immunoreactivity. The tumors were also negative for TH staining, suggesting poor neuronal differentiation. GFAP levels and the absence of TH indicate a poor degree of differentiation, which directly correlates with previous observations on undifferentiated NBL (Wang et al., 2013; Warren et al., 2018). Finally, TUJ1 and S100 staining revealed strong immunoreactivity on 1p36-del/*Mycn* tumors whereas *Mycn*-alone tumors were weakly positive for both markers. Finally, WB analysis of *Arid1a*, *Chd5*, and *Mycn* performed on 1p36-del/Mycn and Mycn tumors showed a drastic reduction of Arid1a protein levels, especially in tumors with reduced tumor latency (Figure 4C). Chd5 protein expression did not show a specific pattern that we could link to tumor latency, and we were able to detect protein expression in all the tumors analyzed (Figure 4C).

NBL Oncogenic Drivers and Altered Pathways

Extensive gene expression profiling of primary NCCs and tumors was carried out to investigate which pathways were promiscuously altered during NCCs transformation. To investigate the mechanisms underlying the reduction in tumor onset, we compared the tumors generated using *Mycn* NCCs (n = 5) with those generated using 1p36-del/*Mycn* NCCs (n = 6). Principal-component analysis (PCA) pinpoints the similarities between both tumor types (Figure S3A). When we further analyzed the expression of *Arid1a*, *Chd5*,

Author Manuscript Author Manuscript Author Manuscript Author Manuscript

and *Mycn*, we observed that *Arid1a* expression was homogeneously reduced in all 1p36-del/*Mycn* tumors in comparison with tumors driven by just *Mycn* overexpression (Figure S3B). *Chd5* did not show a drastic reduction of expression 1p36-del/*Mycn* or *Mycn* tumors, suggesting that *Chd5* loss is not essential to transform NCCs when *Arid1a* and *Mycn* are downregulated and overexpressed, respectively. Interestingly, this confirms the results obtained by WB analysis, in which both 1p36-del/*Mycn* and *Mycn* tumors showed that reduction of Arid1a protein expression below levels of detection is associated with reduced tumor latency even in *Mycn* tumors. Although *Mycn* and 1p36-del/*Mycn* tumors showed similar transcriptomic landscape, we observed a particular subset of genes that presented differential expression profiles potentially related to differences in tumor latency (Figure 5A). Focusing on genes that are in the 1p36 locus, we detected that *Arid1a* was the most significantly downregulated gene in the 1p36 locus ($p < 0.05$) when both tumor types were compared (Figure 5B; Figure S3B). In addition we performed a regression analysis comparing the expression of different 1p36 genes that have been proposed as potential tumor suppressor candidates, including *Arid1a*, *Chd5*, *Camta1*, and *Kif1b*. This analysis allows us to identify whether the loss of expression of different 1p36 genes correlates with reduction of tumor latency. The strongest observable relationship was between *Arid1a* expression levels and time to tumor onset, with a significant correlation of 0.96 (Figure 5C).

Gene set enrichment analysis (GSEA) was performed to focus on the changes of expression between 1p36-del/*Mycn* and *Mycn* tumors. Genes showing differential expression ($p < 0.05$) after comparing both tumor groups were introduced in Enrichr software and tested by an enrichment in transcription factors (TFs) using the datasets included in ENCODE and CHEA databases. Differentially expressed genes were associated with polycomb repressive complex 2 (PRC2) and apoptosis in 1p36-del/Mycn tumors in comparison with *Mycn* tumors (Figures S4A and S4B). A massive downregulation of PRC2 targets (both *Suz12* and *Ezh2* are core components of PRC2) was observed (75 different genes were downregulated in 1p36-del/Mycn tumors in comparison with Mycn tumors). Both *Chd5* and *Arid1a* are known to regulate PRC2 targets. *Chd5* modulates PRC2 targets, and *Arid1a*-containing SWI/SNF complexes activate PRC2-repressed genes. NBL has been shown to be preferentially dependent on components of the PRC2 complex (Chen et al., 2018).

Our model is consistent with a signature of increased expression of MYC targets and reduced expression of PRC2 targets that is found in multiple poorly differentiated adult tumors and in NBL (Ben-Porath et al., 2008; Henrich et al., 2016; Yang et al., 2017).

Key regulators of the *Trp53* pathway were downregulated in 1p36/Mycn tumors. For instance, *Perp* was dramatically reduced (log fold change [FC] = −3.35, $p < 0.05$), whereas *Cyfip2*, a p53 target whose expression is sufficient for caspase activation and cellular apoptosis, was downregulated as well (log FC = −0.92, $p < 0.05$). *Perp* induces nuclear localization and increases the level of transcriptionally active *Trp53*, affecting the equilibrium between *Trp53* and *Mdm2* levels. This suggests that *Perp* and *Cyfip2* downregulation helps *Mycn* overexpression to overcome apoptotic signaling pathways, reducing time to tumor onset in 1p36-del/*Mycn* tumors. Both *Perp* and *Cyfip2* downregulation was confirmed by qRT-PCR analysis along with other genes used to validate the RNA sequencing (RNA-seq) results (Figure S5). On the other hand, we detected an

Author Manuscript Author Manuscript Author Manuscript Author Manuscript

upregulation of genes associated with the Rest TF (Figure S4A). REST protein can act as enhancer or silencer depending on the cellular context (Bessis et al., 1997). Here, we found a cohort of differentially expressed genes that are downstream targets of REST (Figure S4B). Such a REST signature has been previously reported in NBL patients (Liang et al., 2014) and is associated with poor neuronal differentiation in many NBL patient samples and cell lines (Di Toro et al., 2005; Laneve et al., 2010).

In summary, the expression profile analysis demonstrates that 1p36-del/*Mycn* tumors recapitulate many of the features previously reported in human high-risk NBLs. This mouse model recapitulates high-risk NBL comprising 1p36 LOH and *Mycn* amplification.

Whole-Exome Sequencing (WES), Array CGH, and Targeted Sequencing Analysis to Track 1p36 Loss and SNVs in Our *In Vivo* Model

Arid1a was significantly lost during tumor evolution, as found by RNA-seq and WB analysis. Although *Arid1a* was the prominent 1p36 tumor suppressor associated with *Mycn*, we wanted to determine if *Arid1a* was typically lost through larger deletions, which may indicate that there are other supportive 1p36 tumor suppressors in *Mycn*-driven tumorigenesis or if loss of *Arid1a* was sufficient. We therefore assessed tumor DNA for the types of mutations selected for by tumor evolution. To determine which 1p36 region losses were selected for during tumorigenesis *in vivo*, we performed WES, targeted sequencing analysis, using MiSeq as the sequencing platform, and array comparative genomic hybridization (aCGH) in different 1p36-del/*Mycn* tumors as well as in the parental cell lines subcutaneously injected into the animals. In general, WES and aCGH showed the same results but with different sensitivities. The sensitivity for identifying single nucleotide variants through WES and targeted sequencing data is more than 95%–99% (Meynert et al., 2014); however, detection of large indels including large chromosomal losses is challenging, so we also performed aCGH analysis to obtain a broad view of large chromosomal losses. *Arid1a* and *Chd5* indels were clearly identified in all the parental cell lines by means of targeted sequencing and WES analysis, whereas large deletions were absent (Table S1), indicating that probably fewer than 5% of the parental cell lines we implanted had 1p36-del when they were subcutaneously injected. Four of five tumors had cells with 1p36 loss (Table S1). Such tumors had a heterogeneous population of cells where those showing 1p36 loss represented 9%–20% of total tumor mass. Although no patterns between larger deletions and tumor latency were observed, patterns did emerge when large deletions were combined with smaller indels. When both deletions and indels are considered together for all of the tumors, we observed, by regression analysis, a significant correlation of 0.78 between *Arid1a* mutations and tumor onset and a non-significant correlation of 0.22 for *Chd5* (Figures 6A). Similarly, larger 1p36 deletions of either the distal or the proximal regions did not have significant correlations (Figure 6B). As an additional surrogate for 1p36 loss, we interrogated other tumor suppressors that have been implicated in NBL biology, *Kif1b* and *Camta1* from the distal region of 1p36. Loss of these genes as assessed using aCGH (Figure 6B) or RNA-seq (Figure 5C) did not correspond to tumor latency, though we did not interrogate their contribution by directly targeting them. These findings indicate that *Mycn* can achieve more rapid transformation of NCCs when those cells have *Arid1a* deleted, irrespective of whether that loss occurred through indels or large deletions (Figure 6A).

Author Manuscript Author Manuscript Author Manuscript Author Manuscript

We used the NBL cell line SK-N-AS to further explore the functional relationship between *Arid1a* and *Mycn*. SK-N-AS cells are N-Myc WT with a small 1p36 deletion (Fujita et al., 2008). Because of the small size of its deletion, SK-N-AS was important for originally defining the distal 1p36 tumor suppressor region in NBL (Fujita et al., 2008). The SK-N-AS deletion contains all of the currently proposed distal tumor suppressors, including CHD5, but importantly leaves the ARID1A locus intact (White et al., 1995). We engineered SK-N-AS to express MYCN protein (N-Myc) in the presence of doxycycline (Dox) to generate the iN-Myc-AS cell line and used an empty control vector to generate the iCont-AS cell line. Dox-induced expression of N-Myc in iN-Myc-AS cells is equivalent to that seen in the N-Myc-amplified NB cell lines SK-N-BE2 (BE2) and IMR32 (Figure 7A). In addition, stable short hairpin RNA (shRNA) silencing of *Arid1a* was generated in both iN-Myc-AS and iCont-AS cell lines to test whether Arid1a loss can increase the tolerance of SK-N-AS cells to N-Myc overexpression (Figure 7B). Dox-induced expression of N-Myc causes a dramatic reduction in cell numbers in iN-Myc-AS cells after 1 week of treatment at multiple concentrations of Dox (Figure 7C), with loss of cell number starting after 4 days of treatment Figure 7D). Multiple independent shRNAs to *Arid1a* block N-Myc-induced cell loss (Figure 7E). The results in the SK-N-AS cell line demonstrate that deletion of the distal 1p36 tumor suppressor region is not sufficient for cells to tolerate N-Myc overexpression at levels equivalent to MycN-amplified NBL but that silencing of *Arid1a* allows cells to tolerate high levels of N-Myc expression. Our findings highlight the role of *Arid1a* loss as a facilitator in *Mycn*-driven oncogenesis.

DISCUSSION

NBL is a cancer that is prominently characterized by segmental chromosomal gains and losses. Despite the hope of finding therapeutically targetable oncogenic drivers, sequencing of hundreds of NBL genomes has identified few recurrent somatic mutations beyond chromosomal rearrangements, such as loss of 1p36 or gain of 17q (Pugh et al., 2013). In this study, using the detailed genomic analysis of this region in NBL as a guide and using genome editing in normal primary NCCs, we further defined the contribution of 1p36 loss to disease initiation.

In vitro, our findings indicate that loss of the mouse syntenic 1p36 region can block differentiation, maintain higher rates of proliferation under differentiation conditions, and increase migration. Loss of *Chd5* was capable of blocking differentiation and promoting migration to an extent comparable with 1p36 deletion. Interestingly, deletion of *Chd5* caused the most colonies in a colony-forming assay, suggesting that loss of other genes in the 1p36 locus reduces the effects of *Chd5* loss in anchorage-independent growth (Figure 2A). Furthermore, loss of additional tumor suppressors in 1p36 contributes to proliferation, as seen by the significant difference between syntenic 1p36 deletions versus *Chd5* deletions (Figure 2D). In contrast, when *Mycn* was overexpressed to generate tumors, both transcriptional and allelic loss of *Arid1a* significantly corresponded with reduced tumor latency (Figures 4A, 4C, and 6). This identified *Arid1a* as a prominent 1p36 tumor suppressor that collaborates with *Mycn*-mediated transformation of NCCs. From these data, we suggest a model in which loss of the distal region of 1p36 involves multiple NBL tumor suppressors, including *CHD5*, that could collaborate with other common NBL alterations,

Author Manuscript Author Manuscript Author Manuscript Author Manuscript

such as 17q gain, to achieve transformation. However, only 1p36 LOH that includes Arid1a provide significant advantage to *MYCN*-driven oncogenesis, explaining why larger 1p36 deletions associate with *MYCN* amplification.

A recent study identified genetic dependencies of *MYCN*-amplified NBL cell lines for *EZH2*, *EED*, and *SUZ12*, all core components of PRC2 (Chen et al., 2018). Classically, PRC2 acts in opposition to SWI/SNF, with PRC2 repressing and SWI/SNF activating the same target genes. When *ARID1A* is lost, PRC2 complexes would be predicted to suppress genes targeted by the *ARID1A*-containing SWI/SNF complexes. We do observe that the top enriched pathways for downregulated genes from our RNA-seq data comparing *Mycn* with 1p36-del/*Mycn* tumors are targets of *SUZ12* and *EZH2*, both components of PRC2. Our finding that loss of *Arid1a* favors *Mycn*-driven tumorigenesis and the recent finding that *MYCN*-amplified NBL is dependent on PRC2 both suggest a cooperation between PRC2-mediated gene suppression and tolerance for *MYCN* in NBL.

We present an accurate mouse high-risk NBL mouse model that includes 1p36 loss and *Mycn* amplification. This study substantiates previous predictions from NBL genetic studies, which proposed that two tumor suppressor regions exist in 1p36. Our findings suggest that the tumor suppressors in 1p36 that contribute to NBL have roles that are context specific and indicate that large 1p36 deletions allow the simultaneous loss of two tumor suppressors, with one contributing to NBL initiation and the second being permissive for *MYCN* amplification.

STAR★METHODS

LEAD CONTACT AND MATERIALS AVAILABILITY

Please make all requests for reagents to the lead contact: Kevin W. Freeman (kfreem22@uthsc.edu)

There are restrictions to the availability of neural crest cell lines due to the lack of an external centralized repository for its distribution and our need to maintain the stock of non-immortalized cell lines. We are glad to share neural crest cell lines with reasonable compensation by requestor for its processing and shipping.

EXPERIMENTAL MODEL AND SUBJECT DETAILS

Animal Experiments—This study was performed in strict accordance with the recommendations in the Guide for the Care and Use of Laboratory Animals of the National Institute of Health. All animal experiments were approved by the Institutional Animal Care and Use Committee (IACUC) at St. Jude Children's Research Hospital. For subcutaneous tumor experiments, cells were injected into the hind flank of 6–8 week old C57BL/6 female mice (Charles River Laboratories). Three different experimental replicates consisting of NCCs derived from different male or female embryonic isolations were nucleoporated using the CRISPR/CAS9 plasmid to target Arid1a and Chd5 loci. Then, the cells were sorted and subcutaneously injected with or without *Mycn* overexpression. *Mycn* overexpression was achieved though retroviral infection of NCCs with an MSCV-*Mycn*-IRES-GFP construct. Both during retroviral transduction and prior to injection into the flank of the mice, NCCs

Author Manuscript Author Manuscript Author Manuscript Author Manuscript

were cultured in CDM which allowed us to expand the NCCs so we could inject 1.5×10^6 cells per mouse in 100μl total volume. Cells were injected in a 1:1 mix of cells and Matrigel (BD Biosciences) and tumor growth was monitored by measuring the size by digital caliper. Tumor volume was calculated using the formula by ½ × (length × width^2). Mice were sacrificed and tumors isolated when they were at least 1500mm^3 or earlier if ulcerated. We used ten mice per treatment group for NCCs control, 1p36-del NCCs, 1p36/Mycn NCCs and Mycn-alone NCCs. Mice were housed with 4 to 5 mice per cage with corn cob bedding in normal light-dark cycling at room temperature (~23°C). Food and water were provided *ad libitum*. Mice were sacrificed using CO_2 asphyxiation followed by cervical dislocation.

Culture Media and Reagents—Mouse NCCs were growth in CDM (Fukuta et al., 2014), which contains Iscove's modified Dulbecco's medium/Ham's F-12 1τ1, 1X chemically defined lipid concentrate (GIBCO), 1X μg/ml Insulin-transferrin-selenium (Thermo Fisher Scientific), 450 μM monothioglycerol (Sigma), 5 mg/ml purified BSA (Sigma), 7 μg/ml Insulin (Thermo Fisher Scientific), and penicillin/streptomycin (Invitrogen). Culture dishes were coated with fibronectin (250 μg/mL) (Corning). The medium was supplemented with EGF (R&D) and FGF2 (R&D) to modulate growth factor signals and SB431542 (SB) (Sigma) as a TGF-beta signaling pathway suppressor. For differentiation assays the regular CDM medium was replaced with DMEM/F12 supplemented with 1 × N2 supplement, we removed the EGF and FGF growth factors and added 10 ng/ml BDNF, GDNF, NT-3 and NGF (R&D). The medium was changed every 48h.

NCC Culture—Day 9.5 embryos were isolated and dissected to remove the neural tube from a region caudal to the heart to the most caudal somite. The isolated neural tubes were treated with collagenase/dispase in PBS (1mg/mL) for 5 minutes and then placed in DMEM + 10% FBS to stop the collagenase/dispase reaction. Fibronectin pre-coated dishes were rinsed 3 times with PBS 1X. Then, single neural tubes were plated in 96 well plates allowing them to attach to bottom of chamber slides by incubating them at 37°C for 10 minutes. Neural tube explants were cultured in chemically defined medium for 48 hours to allow neural crest cell migration onto the plate before the neural tubes were removed. After neural tube removal the neural crest cells were expanded and transfected in CDM.

METHOD DETAILS

Antibodies—Antibodies used in this study were the following: Actin (1:1000, Santa Cruz, sc-1615), Arid1a (1:1000, Cell Signaling, #12354), Chd5 (1:1000, ThermoFisher Scientific, #PA5-37148), Gfap (1:200, Abcam, ab7260), Ki67 (1:1,000, Abcam, ab15580), N-Myc (1:1000, Cell Signaling, #9405), Synaptophysin (1:100, ThermoFisher Scientific, #RM-9111-S), S100 (1:500, Abcam, ab868), Th (1:250, Millipore, AB152) and Tuj1 (1:1000, Abcam, ab18207).

Plasmids and NCC Transfection—The plasmid containing Mycn cDNA inserted downstream of the MSCV-LTR was gift from Dr. MF Roussel (St. Jude Children's Research Hospital, Memphis TN) (Demeure et al., 2012). After retrovirus production NCCs were transduced 24h before mouse injection. In addition, two different gRNA sequences to target CHD5 (g1:GGGCTCAAGTTCCGCTTCGG; g2:TCTCCCATCGTAGTTGACGA)

Author Manuscript Author Manuscript Author Manuscript Author Manuscript

and ARID1A (g1:GTGATATCCCGCCGAATCAT; g2:GCGGGCTCACGTAGACAGGA) were cloned into an all-in-one pU6-sgRNA-CAS9-P2A-GFP plasmid, which was modified from pX330 (Addgene #42230). Plasmid transfections were performed by electroporation following the manufacturer's instructions (Lonza) to target ARID1A and CHD5 loci.

We established an all-in-one vector system containing several gRNAs, the CAS9 nuclease and one fluorescent marker (GFP or mCherry) all in the same construct. To deliver our vector system into primary mouse NCCs, cells were nucleofected using the Amaxa nucleofection system (Maasho et al., 2004). Then, transfected cells were enriched by FACS and tested for deletions. Since both *Arid1a* and *Chd5* are located in the proximal and distal borders, respectively, of 1p36 mouse syntenic region that we wanted to evaluate, four gRNAs were designed and delivered into the NCCs to target different regions of these genes. WT NCCs used as a control were transfected with empty all-in-one vector just containing the fluorescent marker but not gRNA on it. For all figures WT NCCs label is referring to NCCs transfected with aforementioned empty vector.

CyQuant Assay—In a 96-well tissue culture plate, 5×10^4 cells were plated in 100μl media containing CDM. Plates were incubated for 72 hours and then submitted to CyQuant Cell Direct Proliferation Assay (Thermo Fisher Scientific) according to manufacturer's instructions and read with a Synergy HT Multi-mode microplate reader (Bio-Tek instruments).

FISH Analysis and Karyotyping—Two pairs of probes were developed for FISH analysis. Two were labeled green and targeted flanking regions outside of *Arid1a* and *Chd5*. The other two probes were labeled red and targeted different regions inside of the 1p36-syntenic region upstream and downstream of *Arid1a* and *Chd5* loci, respectively. The results confirmed the achievement of a heterozygous deletion of 1p36. Cells generated from different rounds of nucleofection were evaluated by FISH analysis and varied between 2.5% and 85% for large deletions on mouse chromosome 4. Clonal populations presenting the 20Mb deletion were used to check hallmarks of cell transformation. A FISH assay to detect an engineered deletion of 20 megabases was designed and validated. Two clones located immediately outside of the deleted region on both centromeric and telomeric ends were combined and used as internal control probes; two additional clones located immediately inside the deleted region on both ends were combined used as the test clones. Purified BAC DNAs from the control probes were labeled with AF488 and the test clones with AF594. The control clones were RP23–363D2 and RP23–137L22, and the test clones used were RP23–81J2 and RP24–364D6. The 4 probes were combined and hybridized to interphase and metaphase cells derived from the four samples using routine cytogenetic methods in a solution containing 50% formamide, 10% dextran sulfate, and 2X SCC. The cells were then stained with 4, 6-diamidino-2-phenylindole (DAPI) and analyzed. Two hundred cells were scored for the deletion of the red signals resulting in green signals that are not paired with red indicating a deletion of the targeted region.

The tumor was processed into a single cell suspension and harvested by routine cytogenetic methods after a five hour colcemid exposure time. Additionally, a portion of the single cell suspension was placed in culture for 24 hours and processed in a similar manner. The slides

Author Manuscript Author Manuscript Author Manuscript Author Manuscript

were allowed to air dry for optimal banding of the chromosomes with trypsin and Wright's stain. The banding and morphology were better from the overnight culture and were used in this study.

For karyotyping analysis the cells were harvested by routine cytogenetic methods after a five hour colcemid exposure time. The slides were allowed to air dry for optimal banding of the chromosomes with trypsin and Wright's stain.

RNA-Seq Analysis—Total RNA was extracted from NCCs cells using an RNeasy Plus Mini Kit (QIAGEN). Fastq sequences derived from total RNA paired-end 100 bp sequences were mapped to the mm9 genome with the STAR (Dobin et al., 2013) aligner. Transcript level data were counted using HTSEQ (Anders et al., 2015). Raw counts were voom normalized and contrasted using the empirical Bayes pipeline limma in R 3.2.3 (Law et al., 2014). PCAs were used to quality control data using Partek Genomics Suite 6.6 (St Louis, Mo). Plots were produced using STATA/MP 14.2 (College Station).

Pathway Analysis—Gene-set enrichment analysis was performed through Enrichr (http://amp.pharm.mssm.edu/Enrichr/) using the EnrichR web available tool (Kuleshov et al., 2016). The enrichment was obtained using "ENCODE_and_ChEA_Consensus_TFs_from_ChIP-X" and "ENCODE TF ChIP-seq 2015" as the database option. Unless stated otherwise, the enrichment analysis was performed on the top 200 genes of the sorted gene list based on the adjusted p value score. The rank based ranking is derived from running Fisher exact test.

Whole-Exome Sequencing—Whole exome sequencing was performed at HudsonAlpha Institute for Biotechnology (Huntsville, AL) using Roche-NimbleGen Sequence Capture EZ Exome v2 kit and paired-end 100nt sequencing on the Illumina HiSeq. The sample coverage was 100X for all of them except tumor C1 that was 200X. Samples were quantitated with a HS and BR DNA Qubit kit using 1 ul of a 1X dilution (1 ul sample). Sequencing reads were aligned to a mouse reference sequence (UCSC assembly mm9, NCBI Build 37), the average depth coverage for each targeted region was generated, and genotypes were called on positions at region of interest with high quality sequence bases (Phred-like Q25 or greater), using CLC Genomics Workbench v9.0 (QIAGEN, Denmark). For copy number analysis, all tumor samples were compared to the average of three parental samples, at each targeted region, followed by circular binary segmentation as above mentioned. The gRNA-introduced mutation profiles at Arid1a and Chd5 were further summarized according to the genotype calls against the reference sequence.

Array CGH and Targeted Sequencing—A genome-wide microarray (G4839A, Agilent Mouse CGH 4×180K), consisting of 60-mer *in situ* synthesized oligonucleotides, was designed and manufactured by Agilent Technologies (Santa Clara, CA. This array contained 170,305 probes spaced across the genome. Array hybridization was performed according to the manufacturer's recommended protocols. In brief, genomic DNA was labeled using the Agilent's ULS Labeling kit. Hybridization was carried out in an Agilent oven at 65°C for 40 hours at 20 rpm, followed by standard wash procedures. The microarray was then scanned in an Agilent scanner at 3 μm resolution, and the array data were extracted using

Author Manuscript Author Manuscript Author Manuscript Author Manuscript

the CGH settings with background-subtracted and LOESS normalization of Agilent Feature Extraction Software (v10.5). The circular binary segmentation algorithm (Olshen et al., 2004) implemented in the DNAcopy package from Bioconductor was then applied to the normalized log2 ratio data to identify copy number alterations for each sample.

Genomic DNA was sequenced on a MiSeq System (Illumina, San Diego, CA, USA) in a paired-end mode with 300 cycles per read (2 × 300 base pairs in depth). Raw fragments from the MiSeq sequencer were first preprocessed to remove any trace of PhiX sequence and then trimmed to remove sequencing adapters as well as low quality bases from the 3′ end (using Trimmomatic version 0.32).

Soft Agar Colony Assay and Wound Healing Assay—Soft agar colony assay was performed following the methodology previously described (Borowicz et al., 2014). Briefly, 15000 NCCs were seeded per well on 24-well plates (Corning) and cultured for 31 days. Then, plates were scanned and analyzed for colony detection. Up to 200 different cells/colonies were analyzed on each experimental replicate. Cells that were bigger than 1000 px^2 were considered colonies.

To evaluate cell-cell interactions on cell migration we performed wound healing assays (Rodriguez et al., 2005). We created a “wound” in a cell monolayer and then we monitor the process of closure of aforementioned “wound” by taking images at the beginning of the experiment at 24h and 48h during cell migration. The images were compared to quantify the migration rate of the cells.

Immunostaining—For Immunohistochemistry (IHC) the tumors were fixed in 10X neutral buffered formalin and sectioned (5 μm thick) for subsequent hematoxylin and eosin (H&E) staining and immunohistochemistry (IHC) for the detection of Map2, Gfap, Synaptophysin, Tuj1, S100 and Ki67. The paraffin sections were incubated with biotinylated secondary antibodies (Vector) and signals were amplified by a horseradish peroxidase system (ABC kit, Vector) followed by DAB staining (Sigma-Aldrich).

Immunocytochemistry (ICC) was performed on NCCs to test the expression of different neuronal and proliferation markers as Th, Map2, Tuj1 and Ki67. Cells were fixed with 4% paraformaldehyde in PBS (PFA/PBS) cells were fixed with 4% PFA/PBS for 10 min at room temperature, permeabilized for 5 min in PBS containing 0.25% Triton X-100. Then, cells were subsequently incubated with the primary antibody overnight at 4 °C after blocking with 10% normal donkey serum. Fluorescent images were captured using a confocal laser-scanning microscope (Nikon C2). At least eight sections from one mouse were stained. Cell counting was done in a double-blind manner whenever applicable. Representative images were selected from sections from at least three independent mice.

QUANTIFICATION AND STATISTICAL ANALYSIS

Statistical Analysis—All results were expressed as the mean ± SD unless otherwise indicated. To compare the difference between two groups, the Student’s t test (two tailed) was performed. Colony number was presented as the mean ± standard deviation from three independent experiments. Associations between both tumors types and survival were

Author Manuscript Author Manuscript Author Manuscript Author Manuscript

evaluated by univariate analysis using the log-rank test. Statistical analyses were conducted using Prism 8 (GraphPad Software), except for stratified log-rank survival analyses which were conducted in R (version 3.6.0) using the 'survival' package (version 2.44).

Supplementary Material

Refer to Web version on PubMed Central for supplementary material.

ACKNOWLEDGMENTS

This work was supported by research funds from Department of Defense (DoD) award W81XWH-14-1-0090, DoD grant W81XWH1810477, NIH grant 7R01CA216394-02, American Lebanese Syrian Associated Charities (ALSAC), and the UTHSC Center for Cancer Research.

DATA AND CODE AVAILABILITY

The accession numbers for the RNA sequencing and genome variation profiling by genome tiling array data described in this publication are GEO: GSE123281 and GSE123142 respectively. All data generated during this study are available at (https://www.ncbi.nlm.nih.gov/geo/).

REFERENCES

Anders S, Pyl PT, and Huber W (2015). HTSeq—a Python framework to work with high-throughput sequencing data. Bioinformatics 31, 166–169. [PubMed: 25260700]

Bagchi A, and Mills AA (2008). The quest for the 1p36 tumor suppressor. Cancer Res. 68, 2551–2556. [PubMed: 18413720]

Bagchi A, Papazoglu C, Wu Y, Capurso D, Brodt M, Francis D, Bredel M, Vogel H, and Mills AA (2007). CHD5 is a tumor suppressor at human 1p36. Cell 128, 459–475. [PubMed: 17289567]

Barbashina V, Salazar P, Holland EC, Rosenblum MK, and Ladanyi M (2005). Allelic losses at 1p36 and 19q13 in gliomas: correlation with histologic classification, definition of a 150-kb minimal deleted region on 1p36, and evaluation of CAMTA1 as a candidate tumor suppressor gene. Clin. Cancer Res 11, 1119–1128. [PubMed: 15709179]

Ben-Porath I, Thomson MW, Carey VJ, Ge R, Bell GW, Regev A, and Weinberg RA (2008). An embryonic stem cell-like gene expression signature in poorly differentiated aggressive human tumors. Nat. Genet 40, 499–507. [PubMed: 18443585]

Beroukhim R, Mermel CH, Porter D, Wei G, Raychaudhuri S, Donovan J, Barretina J, Boehm JS, Dobson J, Urashima M, et al. (2010). The landscape of somatic copy-number alteration across human cancers. Nature 463, 899–905. [PubMed: 20164920]

Bessis A, Champtiaux N, Chatelin L, and Changeux JP (1997). The neuron-restrictive silencer element: a dual enhancer/silencer crucial for patterned expression of a nicotinic receptor gene in the brain. Proc. Natl. Acad. Sci. U S A 94, 5906–5911. [PubMed: 9159173]

Borowicz S, Van Scoyk M, Avasarala S, Karuppusamy Rathinam MK, Tauler J, Bikkavilli RK, and Winn RA (2014). The soft agar colony formation assay. J. Vis. Exp (92), e51998. [PubMed: 25408172]

Brodeur GM (2003). Neuroblastoma: biological insights into a clinical enigma. Nat. Rev. Cancer 3, 203–216. [PubMed: 12612655]

Carén H, Fransson S, Ejeskär K, Kogner P, and Martinsson T (2007). Genetic and epigenetic changes in the common 1p36 deletion in neuroblastoma tumours. Br. J. Cancer 97, 1416–1424. [PubMed: 17940511]

Author Manuscript Author Manuscript Author Manuscript Author Manuscript

Caron H, Spieker N, Godfried M, Veenstra M, van Sluis P, de Kraker J, Voûte P, and Versteeg R (2001). Chromosome bands 1p35–36 contain two distinct neuroblastoma tumor suppressor loci, one of which is imprinted. Genes Chromosomes Cancer 30, 168–174. [PubMed: 11135433]

Chen L, Alexe G, Dharia NV, Ross L, Iniguez AB, Conway AS, Wang EJ, Veschi V, Lam N, Qi J, et al. (2018). CRISPR-Cas9 screen reveals a MYCN-amplified neuroblastoma dependency on EZH2. J. Clin. Invest 128, 446–462. [PubMed: 29202477]

Cheng NC, Van Roy N, Chan A, Beitsma M, Westerveld A, Speleman F, and Versteeg R (1995). Deletion mapping in neuroblastoma cell lines suggests two distinct tumor suppressor genes in the 1p35–36 region, only one of which is associated with N-myc amplification. Oncogene 10, 291–297. [PubMed: 7838528]

Cheung NK, and Dyer MA (2013). Neuroblastoma: developmental biology, cancer genomics and immunotherapy. Nat. Rev. Cancer 13, 397–411. [PubMed: 23702928]

Cho HD, Lee JE, Jung HY, Oh MH, Lee JH, Jang SH, Kim KJ, Han SW, Kim SY, Kim HJ, et al. (2015). Loss of tumor suppressor ARID1A protein expression correlates with poor prognosis in patients with primary breast cancer. J. Breast Cancer 18, 339–346. [PubMed: 26770240]

Demeure O, Filangi O, Elsen JM, and Le Roy P (2012). Comparison of the analyses of the XVth QTLMAS common dataset II: QTL analysis. BMC Proc. 6 (Suppl 2), S2.

Di Toro R, Baiula M, and Spampinato S (2005). Expression of the repressor element-1 silencing transcription factor (REST) is influenced by insulin-like growth factor-I in differentiating human neuroblastoma cells. Eur. J. Neurosci 21, 46–58. [PubMed: 15654842]

Dobin A, Davis CA, Schlesinger F, Drenkow J, Zaleski C, Jha S, Batut P, Chaisson M, and Gingeras TR (2013). STAR: ultrafast universal RNA-seq aligner. Bioinformatics 29, 15–21. [PubMed: 23104886]

Fujita T, Igarashi J, Okawa ER, Gotoh T, Manne J, Kolla V, Kim J, Zhao H, Pawel BR, London WB, et al. (2008). CHD5, a tumor suppressor gene deleted from 1p36.31 in neuroblastomas. J. Natl. Cancer Inst 100, 940–949. [PubMed: 18577749]

Fukuta M, Nakai Y, Kirino K, Nakagawa M, Sekiguchi K, Nagata S, Matsumoto Y, Yamamoto T, Umeda K, Heike T, et al. (2014). Derivation of mesenchymal stromal cells from pluripotent stem cells through a neural crest lineage using small molecule compounds with defined media. PLoS ONE 9, e112291. [PubMed: 25464501]

Godfried MB, Veenstra M, Valent A, Sluis Pv., Voûte PA, Versteeg R, and Caron HN (2002). Lack of interstitial chromosome 1p deletions in clinically-detected neuroblastoma. Eur. J. Cancer 38, 1513–1519. [PubMed: 12110498]

Hanahan D, and Weinberg RA (2011). Hallmarks of cancer: the next generation. Cell 144, 646–674. [PubMed: 21376230]

Henrich KO, Schwab M, and Westermann F (2012). 1p36 tumor suppression—a matter of dosage? Cancer Res. 72, 6079–6088. [PubMed: 23172308]

Henrich KO, Bender S, Saadati M, Dreidax D, Gartlgruber M, Shao C, Herrmann C, Wiesenfarth M, Parzonka M, Wehrmann L, et al. (2016). Integrative genome-scale analysis identifies epigenetic mechanisms of transcriptional deregulation in unfavorable neuroblastomas. Cancer Res. 76, 5523–5537. [PubMed: 27635046]

Huang X, and Saint-Jeannet JP (2004). Induction of the neural crest and the opportunities of life on the edge. Dev. Biol 275, 1–11. [PubMed: 15464568]

Huang M, and Weiss WA (2013). Neuroblastoma and MYCN. Cold Spring Harb. Perspect. Med 3, a014415.

Jiang ZH, Dong XW, Shen YC, Qian HL, Yan M, Yu ZH, He HB, Lu CD, and Qiu F (2015). DNA damage regulates ARID1A stability via SCF ubiquitin ligase in gastric cancer cells. Eur. Rev. Med. Pharmacol. Sci 19, 3194–3200. [PubMed: 26400522]

Kuleshov MV, Jones MR, Rouillard AD, Fernandez NF, Duan Q, Wang Z, Koplev S, Jenkins SL, Jagodnik KM, Lachmann A, et al. (2016). Enrichr: a comprehensive gene set enrichment analysis web server 2016 update. Nucleic Acids Res. 44 (W1), W90–W97. [PubMed: 27141961]

Laneve P, Gioia U, Andriotto A, Moretti F, Bozzoni I, and Caffarelli E (2010). A minicircuitry involving REST and CREB controls miR-9–2 expression during human neuronal differentiation. Nucleic Acids Res. 38, 6895–6905. [PubMed: 20624818]

Author Manuscript Author Manuscript Author Manuscript Author Manuscript

Langmead B, and Salzberg S (2012). Fast gapped-read alignment with Bowtie 2. Nature Methods 9 (4), 357–359, In press. [PubMed: 22388286]

Law CW, Chen Y,Shi W,and Smyth GK (2014). voom: precision weights unlock linear model analysis tools for RNA-seq read counts. Genome Biol. 15, R29. [PubMed: 24485249]

Liang J, Tong P, Zhao W, Li Y, Zhang L, Xia Y, and Yu Y (2014). The REST gene signature predicts drug sensitivity in neuroblastoma cell lines and is significantly associated with neuroblastoma tumor stage. Int. J. Mol. Sci 15, 11220–11233. [PubMed: 24968265]

Maasho K, Marusina A, Reynolds NM, Coligan JE, and Borrego F (2004). Efficient gene transfer into the human natural killer cell line, NKL, using the Amaxa nucleofection system. J. Immunol. Methods 284, 133–140. [PubMed: 14736423]

Maris JM, Guo C, Blake D, White PS, Hogarty MD, Thompson PM, Rajalingam V, Gerbing R, Stram DO, Matthay KK, et al. (2001). Comprehensive analysis of chromosome 1p deletions in neuroblastoma. Med. Pediatr. Oncol 36, 32–36. [PubMed: 11464900]

Meynert AM, Ansari M, FitzPatrick DR, and Taylor MS (2014). Variant detection sensitivity and biases in whole genome and exome sequencing. BMC Bioinformatics 15, 247. [PubMed: 25038816]

Mosse YP, Greshock J, Margolin A, Naylor T, Cole K, Khazi D, Hii G, Winter C, Shahzad S, Asziz MU, et al. (2005). High-resolution detection and mapping of genomic DNA alterations in neuroblastoma. Genes Chromosomes Cancer 43, 390–403. [PubMed: 15892104]

Nakane Y, Natsume A, Wakabayashi T, Oi S, Ito M, Inao S, Saito K, and Yoshida J (2007). Malignant transformation-related genes in meningiomas: allelic loss on 1p36 and methylation status of p73 and RASSF1A. J. Neurosurg 107, 398–404. [PubMed: 17695396]

Olsen RR, Otero JH, García-López J, Wallace K, Finkelstein D, Rehg JE, Yin Z, Wang YD, and Freeman KW (2017). MYCN induces neuroblastoma in primary neural crest cells. Oncogene 36, 5075–5082. [PubMed: 28459463]

Olshen AB, Venkatraman ES, Lucito R, and Wigler M (2004). Circular binary segmentation for the analysis of array-based DNA copy number data. Biostatistics 5, 557–572. [PubMed: 15475419]

Pikor L, Thu K, Vucic E, and Lam W (2013). The detection and implication of genome instability in cancer. Cancer Metastasis Rev. 32, 341–352. [PubMed: 23633034]

Poetsch M, Dittberner T, and Woenckhaus C (2003). Microsatellite analysis at 1p36.3 in malignant melanoma of the skin: fine mapping in search of a possible tumour suppressor gene region. Melanoma Res. 13, 29–33. [PubMed: 12569282]

Pugh TJ, Morozova O, Attiyeh EF, Asgharzadeh S, Wei JS, Auclair D, Carter SL, Cibulskis K, Hanna M, Kiezun A, et al. (2013). The genetic landscape of high-risk neuroblastoma. Nat. Genet 45, 279–284. [PubMed: 23334666]

Rodriguez LG, Wu X, and Guan JL (2005). Wound-healing assay. Methods Mol. Biol 294, 23–29. [PubMed: 15576902]

Sausen M, Leary RJ, Jones S, Wu J, Reynolds CP, Liu X, Blackford A, Parmigiani G, Diaz LA Jr., Papadopoulos N, et al. (2013). Integrated genomic analyses identify ARID1A and ARID1B alterations in the childhood cancer neuroblastoma. Nat. Genet 45, 12–17. [PubMed: 23202128]

Scaruffi P, Parodi S, Mazzocco K, Defferrari R, Fontana V, Bonassi S, and Tonini GP (2004). Detection of MYCN amplification and chromosome 1p36 loss in neuroblastoma by cDNA microarray comparative genomic hybridization. Mol. Diagn 8, 93–100. [PubMed: 15527323]

Schneider C, Rasband W, and Eliceiri K (2012). NIH Image to ImageJ: 25 years of image analysis. Nature Methods 9 (7), 671–675, In press. [PubMed: 22930834]

Shimada H, Ambros IM, Dehner LP, Hata J, Joshi VV, Roald B, Stram DO, Gerbing RB, Lukens JN, Matthay KK, and Castleberry RP (1999). The International Neuroblastoma Pathology Classification (the Shimada system). Cancer 86, 364–372. [PubMed: 10421273]

Spieker N, Beitsma M, Van Sluis P, Chan A, Caron H, and Versteeg R (2001). Three chromosomal rearrangements in neuroblastoma cluster within a 300-kb region on 1p36.1. Genes Chromosomes Cancer 31, 172–181. [PubMed: 11319804]

Teitz T, Stanke JJ, Federico S, Bradley CL, Brennan R, Zhang J, Johnson MD, Sedlacik J, Inoue M, Zhang ZM, et al. (2011). Preclinical models for neuroblastoma: establishing a baseline for treatment. PLoS ONE 6, e19133. [PubMed: 21559450]

Author Manuscript Author Manuscript Author Manuscript Author Manuscript

Tews B, Felsberg J, Hartmann C, Kunitz A, Hahn M, Toedt G, Neben K, Hummerich L, von Deimling A, Reifenberger G, and Lichter P (2006). Identification of novel oligodendroglioma-associated candidate tumor suppressor genes in 1p36 and 19q13 using microarray-based expression profiling. Int. J. Cancer 119, 792–800. [PubMed: 16550607]

Wang B, Niu D, Lai L, and Ren EC (2013). p53 increases MHC class I expression by upregulating the endoplasmic reticulum aminopeptidase ERAP1. Nat. Commun 4, 2359. [PubMed: 23965983]

Warren M, Matsuno R, Tran H, and Shimada H (2018). Utility of Phox2b immunohistochemical stain in neural crest tumours and non-neural crest tumours in paediatric patients. Histopathology 72, 685–696. [PubMed: 28986989]

Wei XL, Wang DS, Xi SY, Wu WJ, Chen DL, Zeng ZL, Wang RY, Huang YX, Jin Y, Wang F, et al. (2014). Clinicopathologic and prognostic relevance of ARID1A protein loss in colorectal cancer. World J. Gastroenterol 20, 18404–18412. [PubMed: 25561809]

White PS, Maris JM, Beltinger C, Sulman E, Marshall HN, Fujimori M, Kaufman BA, Biegel JA, Allen C, Hilliard C, et al. (1995). A region of consistent deletion in neuroblastoma maps within human chromosome 1p36.2–36.3. Proc. Natl. Acad. Sci. U S A 92, 5520–5524. [PubMed: 7777541]

White PS, Thompson PM, Seifried BA, Sulman EP, Jensen SJ, Guo C, Maris JM, Hogarty MD, Allen C, Biegel JA, et al. (2001). Detailed molecular analysis of 1p36 in neuroblastoma. Med. Pediatr. Oncol 36, 37–41. [PubMed: 11464901]

Yang XH, Tang F, Shin J, and Cunningham JM (2017). Incorporating genomic, transcriptomic and clinical data: a prognostic and stem cell-like MYC and PRC imbalance in high-risk neuroblastoma. BMC Syst. Biol 11 (Suppl 5), 92. [PubMed: 28984200]

Yu F, Gao W, Yokochi T, Suenaga Y, Ando K, Ohira M, Nakamura Y, and Nakagawara A (2014). RUNX3 interacts with MYCN and facilitates protein degradation in neuroblastoma. Oncogene 33, 2601–2609. [PubMed: 23851507]

Zack TI, Schumacher SE, Carter SL, Cherniack AD, Saksena G, Tabak B, Lawrence MS, Zhsng CZ, Wala J, Mermel CH, et al. (2013). Pan-cancer patterns of somatic copy number alteration. Nat. Genet 45, 1134–1140. [PubMed: 24071852]

Author Manuscript Author Manuscript Author Manuscript Author Manuscript

Highlights

- Larger 1p36 deletions involving *Arid1a* locus reduce tumor latency in *Mycn*-driven NBL
- The latency reduction is associated with a deregulation of *PRC2* and *Trp53* pathways
- *Arid1a* loss is favored over other 1p36 candidates in *Mycn*-driven tumors

Author Manuscript Author Manuscript Author Manuscript Author Manuscript

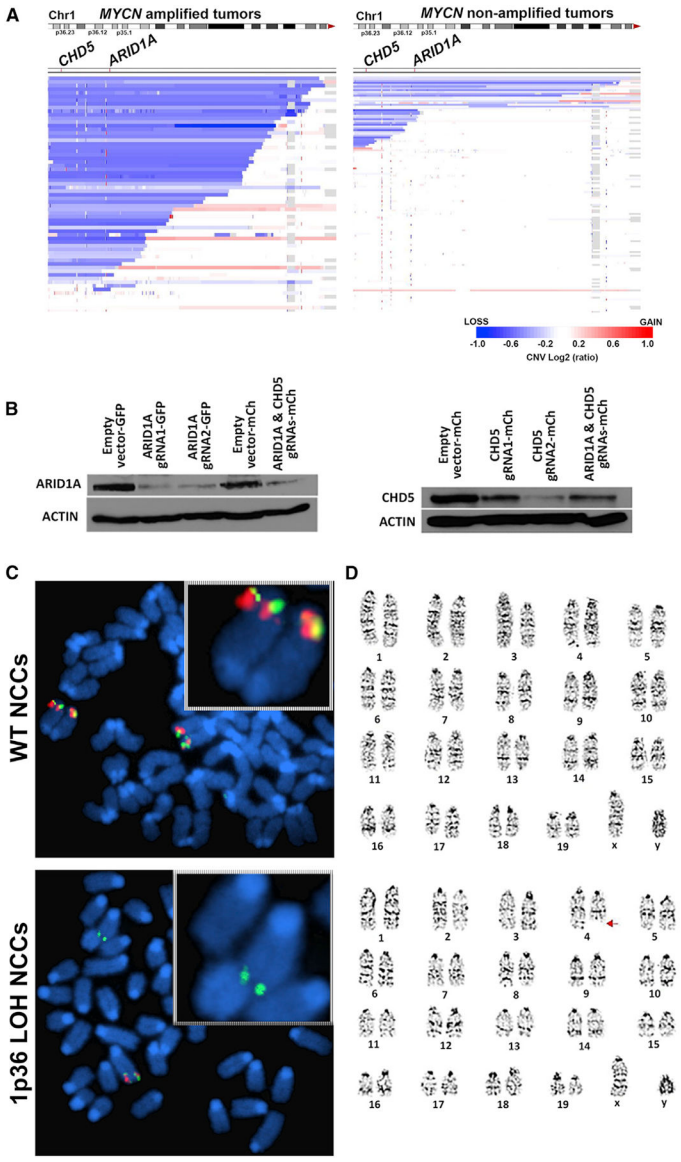

Figure 1. Characterization of 1p36-del-Derived Cell Lines

(A) TARGET data from whole-exome and whole-genome sequencing were segregated on the basis of *MYCN* amplification status and then mapped for 1p36 deletions. Horizontal bars indicate regions of loss (blue) or gain (red).

(B) WB analysis demonstrating the different efficiency of the gRNAs designed to target ARID1A and CHD5.

(C) FISH analysis illustrates the loss of internal clones (red probes) on NCCs that were transfected with our CRISPR/CAS9 constructs.

(D) Karyotyping analysis shows a deletion on chromosome 4 (red arrow) of NCCs engineered through CRISPR/CAS9 technology.

Author Manuscript Author Manuscript Author Manuscript Author Manuscript

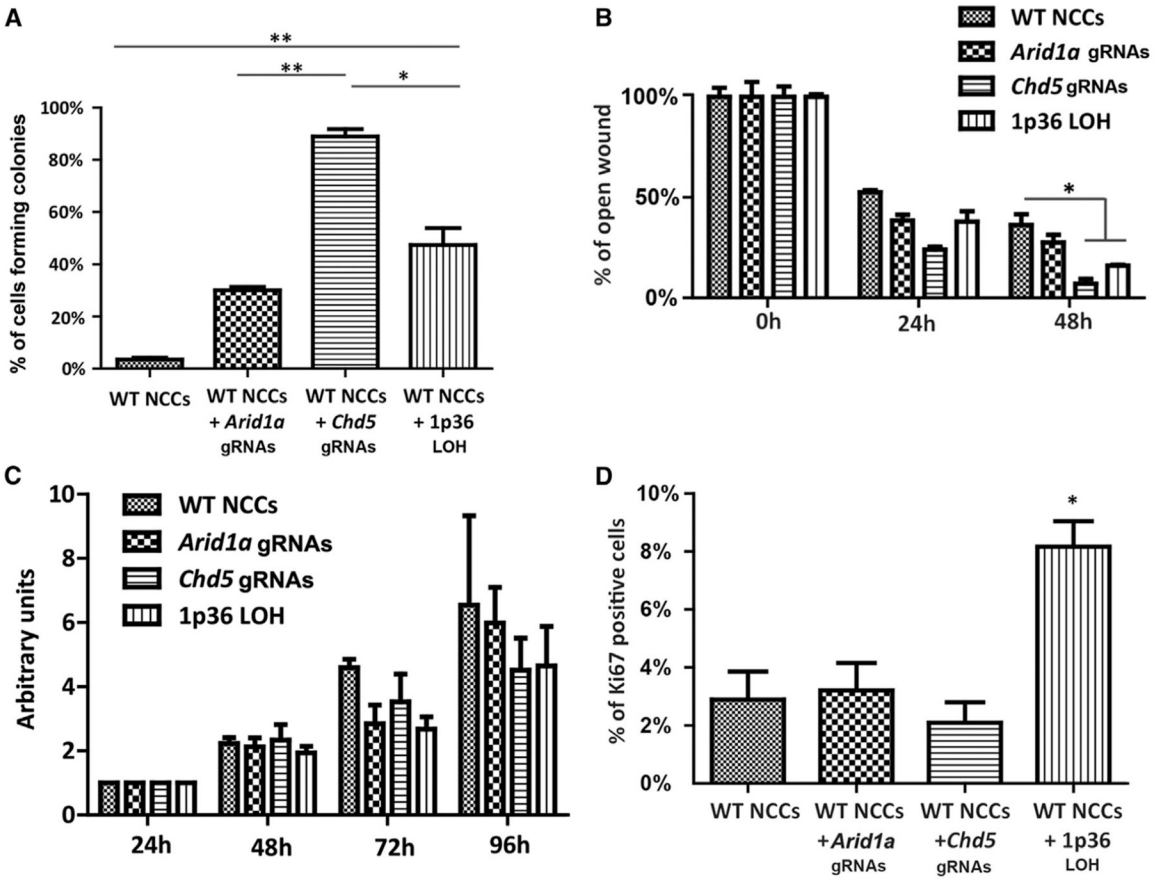

Figure 2. Genetically Engineered NCCs Showed Tumorigenic Capabilities *In Vitro*

(A) Cells with 1p36 or Chd5 deletions increased the number of colonies in soft agar colony formation assay (*p ≤ 0.05 and **p ≤ 0.01).

(B) A wound healing assay was performed in cell lines, with 24 and 48 h of recovery. The images and graphs illustrate that 1p36 or Chd5 deletion stimulated cell migration in both cell lines. Colony number and size are presented as mean ± standard deviation from three independent experiments, and significant differences were determined using Student's t test (*p ≤ 0.05).

(C) Proliferative rates were calculated using the CyQuant assay and are provided as relative fluorescence.

(D) Analysis of mitotic index and Ki67 staining in genetically engineered NCCs. The cells were cultured 7 days in differentiation medium, and Ki67-positive cells were counted per visual field (VF). Results from quantitative cell count analysis of mitotic cells are shown as the percentage of positive cells. Data are presented as mean ± SEM and were analyzed using Student's t test. A p value of less than 0.05 is considered to indicate statistical significance (*p ≤ 0.05).

Author Manuscript Author Manuscript Author Manuscript Author Manuscript

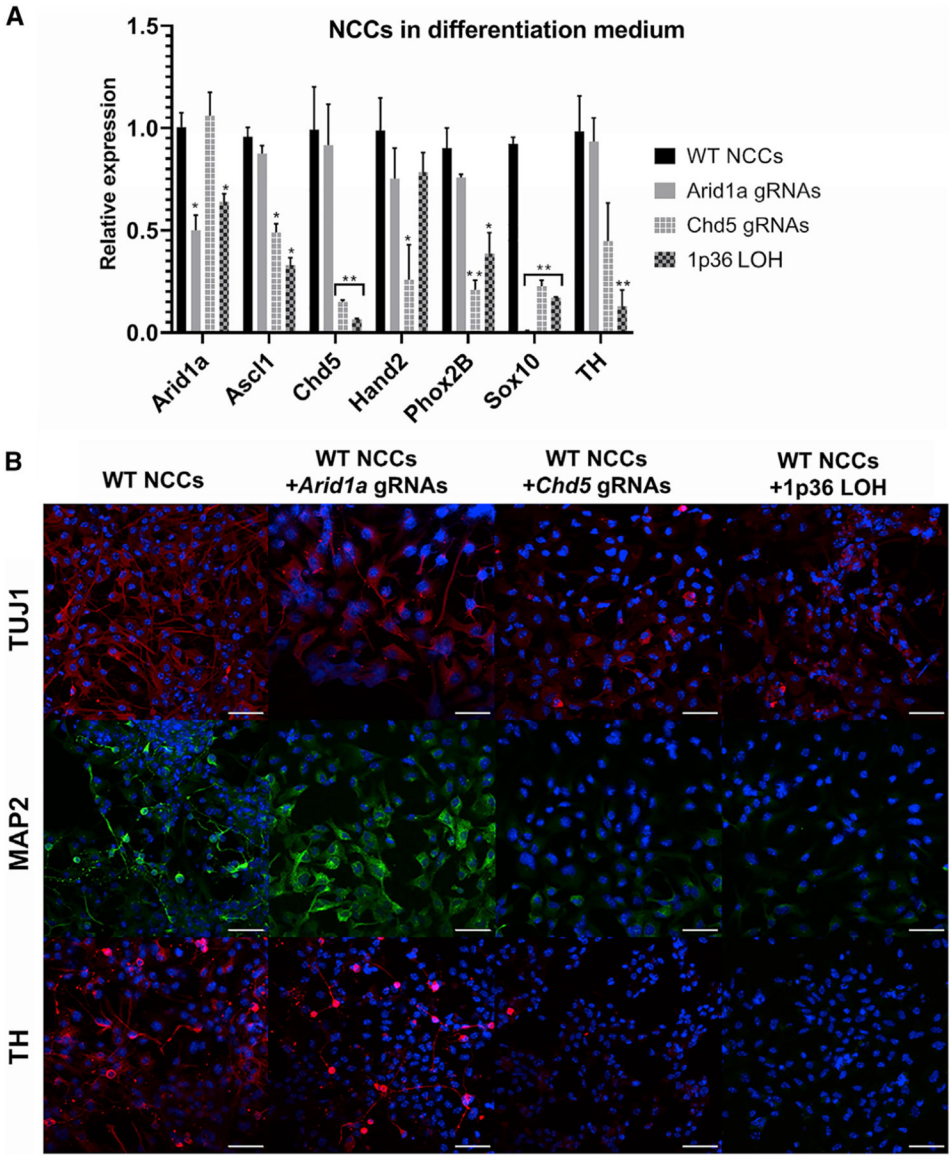

Figure 3. Genetically Engineered NCCs Present Differentiation Impairment *In Vitro*

(A) qRT-PCR analysis of different neuronal markers on genetically engineered NCCs. Differences in gene expression were considered statistically significant after calculation of the p value from a two-way ANOVA for each gene (*$p < 0.05$ and **$p<0.001$). Data are presented as mean ± SEM.

(B) Immunofluorescence (IF) analysis of neuronal markers. Bright-field images show differences between the engineered NCCs and the fluorescence images, with several differentiation markers confirming the impairment of differentiation in 1p36-depleted and CHD5-depleted NCCs. The cells were stained for the nucleus with DAPI (blue) and with the neuronal markers TUJ1 (red), MAP2 (green), and TH (red). Scale bars: 50 μm.

Author Manuscript Author Manuscript Author Manuscript Author Manuscript

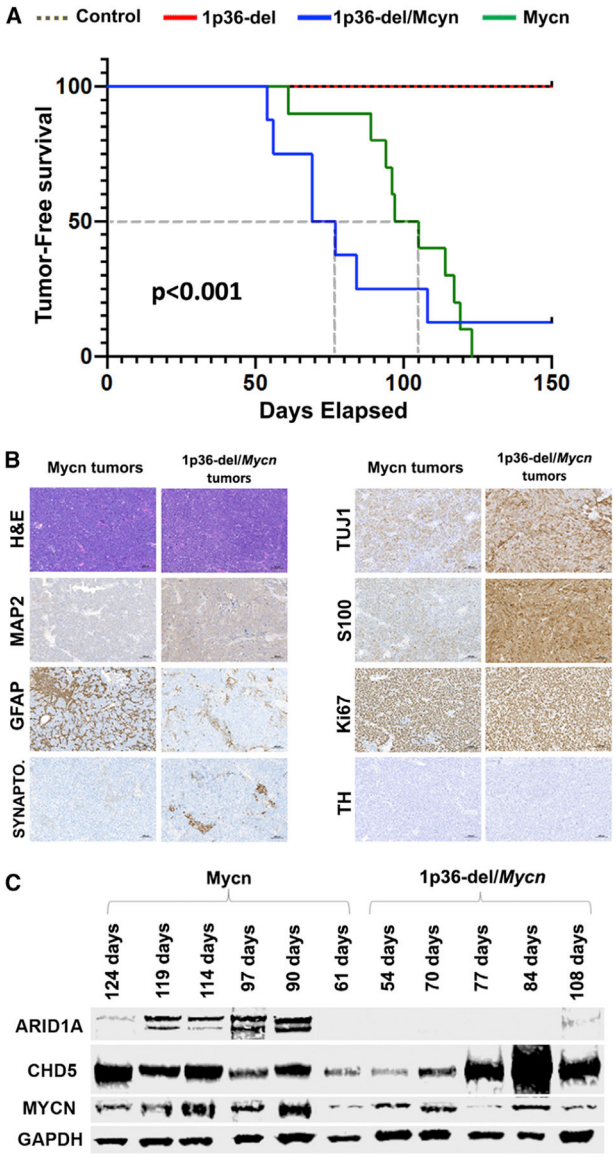

Figure 4. *In Vivo* Tumor Studies

(A) Diagram showing the different engineered NCC populations subcutaneously injected for tumor-onset studies. The Kaplan-Meier tumor-free survival curves show the different timing of tumor onset for different engineered NCCs. Tumor-free survival of mice injected with 1p36/Mycn NCCs was significantly shorter ($p < 0.001$) than that of mice injected with just *Mycn*-overexpressing cells. The log rank test was used to compare survival curves of two groups.

(B) Immunohistochemically analysis of tumor differentiation markers. The tumors that developed after 1p36-del/*Mycn* NCC injection showed increased expression of TUJ1 and S100 staining, whereas Mycn-alone-derived tumors showed an increase of glial cells.

(C) Western blot analysis from protein extracts corresponding to Mycn and 1p36-del/*Mycn* tumors presenting different tumor onset.

Author Manuscript Author Manuscript Author Manuscript Author Manuscript

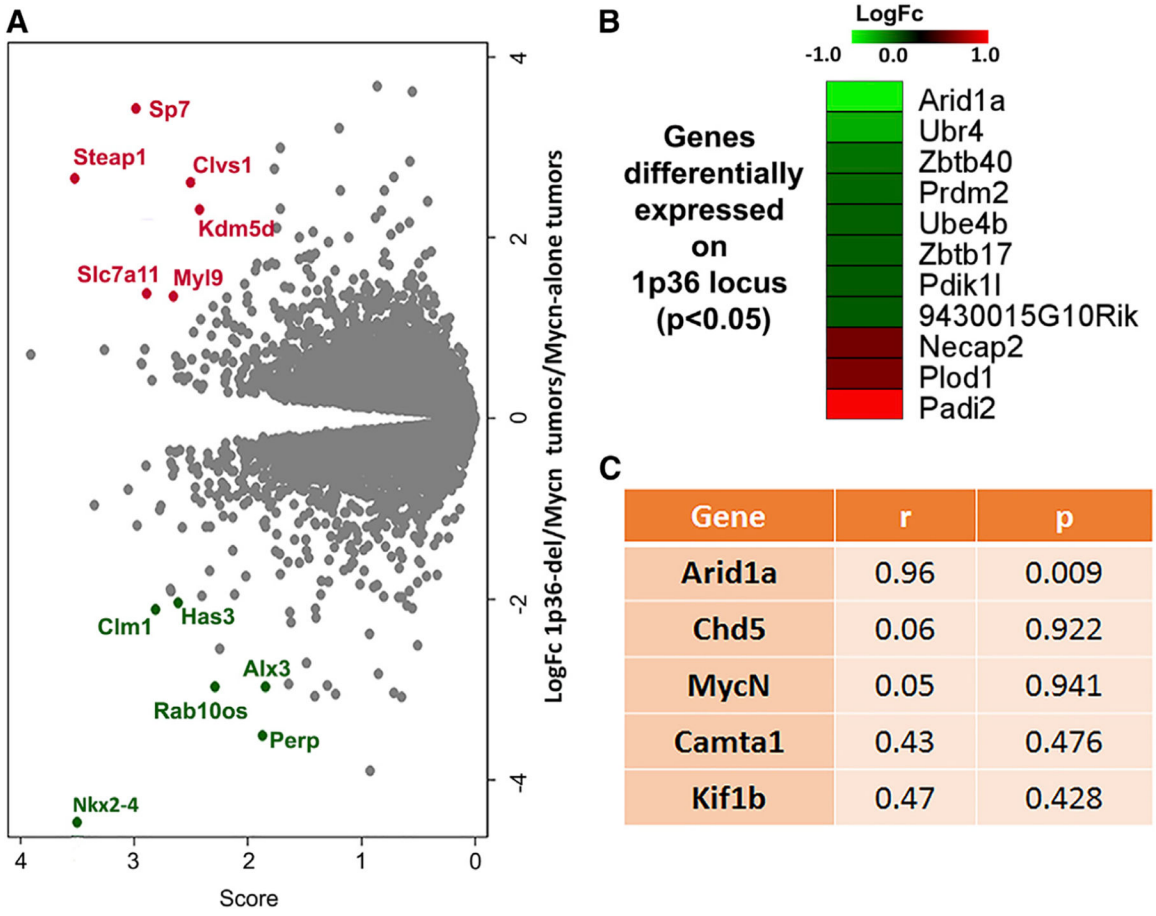

Gene	r	p
Arid1a	0.96	0.009
Chd5	0.06	0.922
MycN	0.05	0.941
Camta1	0.43	0.476
Kif1b	0.47	0.428

Figure 5. RNA-Seq Analysis

(A) Volcano plot comparing the tumors obtained after the injection of *Mycn* NCCs and 1p36/*Mycn* NCCs. Green symbols indicate genes that were significantly downregulated, while red symbols indicate genes that were significantly upregulated in 1p36/Mycn tumors. (B) Heatmap showing the expression of genes included in the 1p36 mouse syntenic region. (C) Correlations between time to tumor onset and RNA-seq expression of *Mycn* and NBL tumor suppressor gene candidates from the distal and proximal regions. Correlation (r) values and p values were determined using linear regression analysis.

Author Manuscript Author Manuscript Author Manuscript Author Manuscript

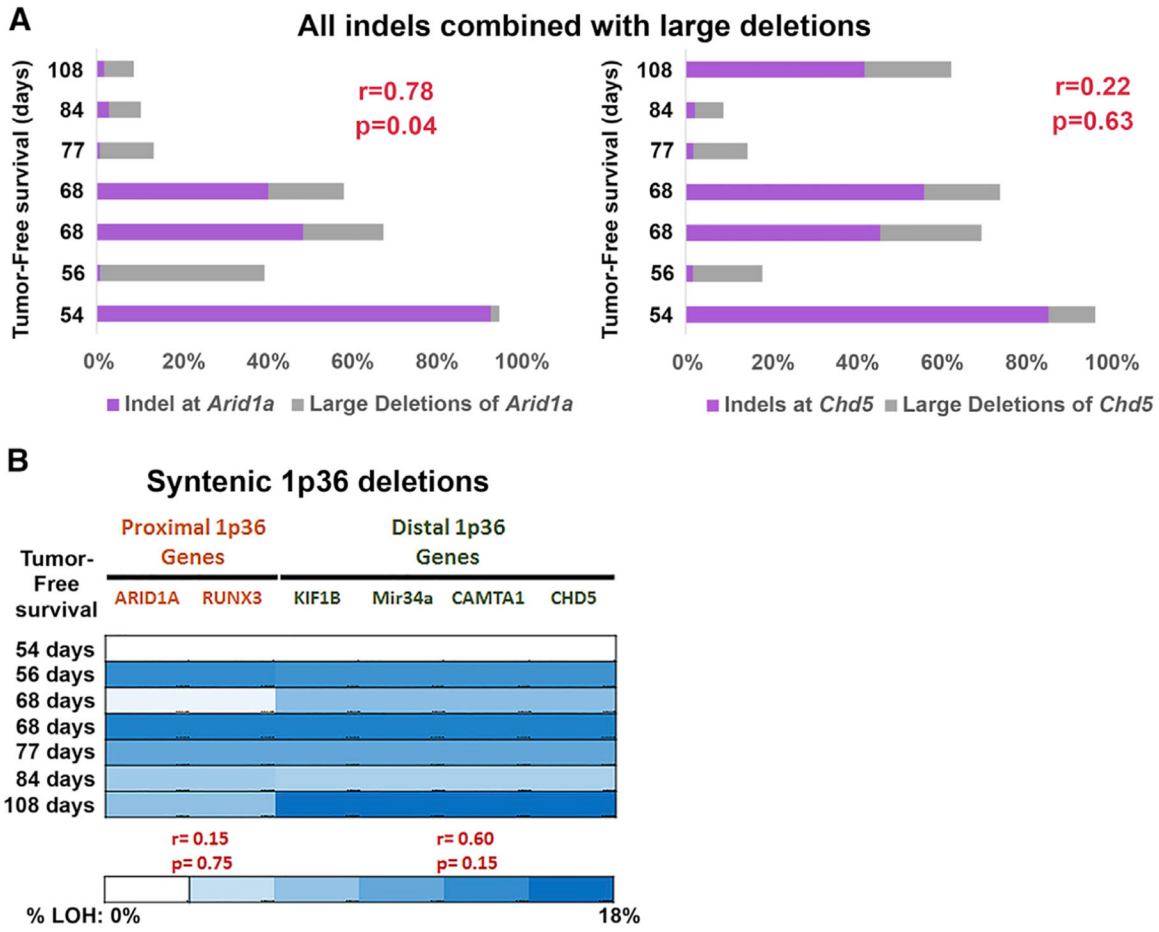

Figure 6. *Arid1a* Loss Significantly Correlates with the Reduction in N-Myc-Driven Tumor Latency

(A) Bar plots representing the correlation between tumor-free survival (in days) with Arid1a and Chd5 loss as combined loss from indels and larger deletions. The analysis illustrates the recurrence of Arid1a loss in tumors presenting the earliest onset.

(B) The time to tumor onset compared with large deletions as determined using aCGH at proposed NBL tumor suppressor genes that are located in the proximal tumor suppressor region (Arid1a and Runx3) and the distal tumor suppressor region (*Kif1b*, *Mir34a*, *Camta1*, and *Chd5*).

Author Manuscript Author Manuscript Author Manuscript Author Manuscript

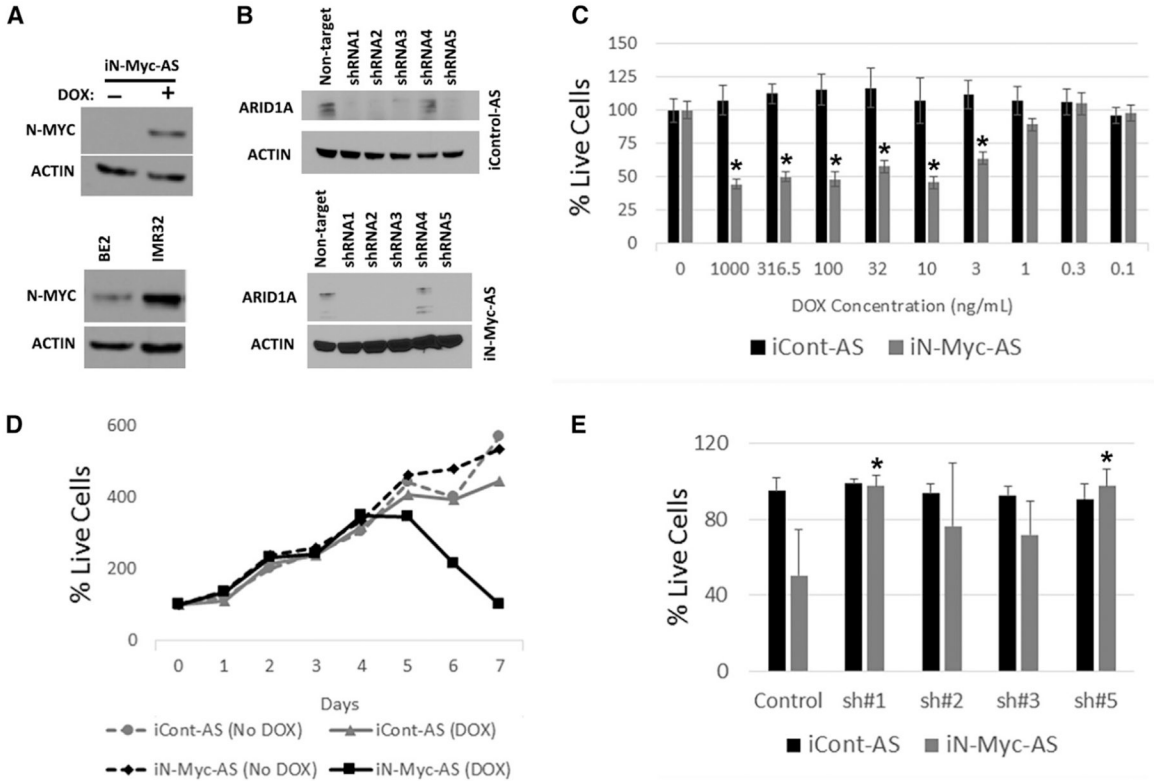

Figure 7. The Intolerance of SK-N-AS Cells for N-Myc Expression Is Reversed by Silencing ARID1A

Stable SK-N-AS cell lines were generated with either Dox-inducible N-Myc expression (iN-Myc-AS) or empty vector control (iCont-AS).

(A) Dox-induced N-Myc in SK-N-AS iN-Myc-AS cell line shows induced N-Myc expression comparable with two MYCN-amplified NBL cell lines, SK-N-BE2 and IMR32, by western blot.

(B) WB analysis of stable iN-Myc-AS and iCont-AS cell lines expressing shRNAs to target *Arid1a*.

(C) Percentage live cells was enumerated at day 7 over a dose range of Dox for iN-Myc-AS or iCont-AS ($n = 3$, $^*p < 0.001$).

(D) Dox-induced N-Myc expression caused cell loss over time at a 100 ng/mL concentration of Dox.

(E) Stable cell lines expressing either scramble shRNA (shRNA cont.) or five different shRNAs to target ARID1A tolerate 1 week of Dox-induced N-Myc expression ($n = 4$, $^*p < 0.05$). Data are presented as mean ± SEM and were analyzed using Student's t test.

Author Manuscript Author Manuscript Author Manuscript Author Manuscript

KEY RESOURCES TABLE

REAGENT or RESOURCE	SOURCE	IDENTIFIER
Antibodies		
Actin	Santa Cruz	Cat# sc-1615; RRID: AB_630835
Arid1a	Cell Signaling	Cat#12354; RRID: AB_2637010
Chd5	ThermoFisher Scientific	Cat# PA5–37148; RRID: AB_2553931
Gfap	Abcam	Cat# ab7260; RRID: AB_305808
Ki67	Abcam	Cat# ab15580; RRID: AB_805388
N-Myc	Cell Signaling	Cat #9405; RRID: AB_10692664
Synaptophysin	ThermoFisher Scientific	Cat#RM-9111-S; RRID: AB_149937
Th	Millipore	Cat#AB152; RRID: AB_390204
S100	Abcam	Cat#ab868; RRID: AB_306716
Tuj1	Abcam	Cat#ab18207; RRID: AB_444319
Biological Samples		
Neural crest cells	Primary cells	Neural tube e9.5
Critical Commercial Assays		
Nucleofector 2b	Lonza	AAB1001
Amaxa Rat NSC Nucleofector kit	Lonza	VPG-1005
CyQuant Cell Direct Proliferation Assay	Thermo Fisher Scientific	C7026
Deposited Data		
RNaseq data	NCBI	GSE123281
Whole exon sequencing Array CGH and targeted deep sequencing	NCBI	GSE123142
Experimental Models: Cell Lines		
SK-N-AS	ATCC®	CRL-2137
N-BE2	ATCC®	CRL-2271
IMR32	ATCC®	CCL-127
Experimental Models: Organisms/Strains		
C57BL/6J mouse embryos from both sexes were utilized to isolate NCCs	Jackson laboratory	
Oligonucleotides		
Chd5 gRNA sequence 1: GGGCTCAAGTTCCGCTTCGG	This paper	N/A
Chd5 gRNA sequence 2: TCTCCCATCGTAGTTGACGA	This paper	N/A
Arid1a gRNA sequence 1: GTGATATCCCGCCGAATCAT	This paper	N/A
Arid1a gRNA sequence 2: GCGGGCTCACGTAGACAGGA	This paper	N/A
Primer *Arid1a* forward: cagcaaccacagcttcagtc	This paper	N/A
Primer *Arid1a* reverse: gctgggagggatatggagtt	This paper	N/A
Primer *Ascl1* forward: gctctcctgggaatggactt	This paper	N/A
Primer *Ascl1* reverse: tcgttggcgagaaacactaa	This paper	N/A
Primer *Chd5* forward: ggggaaaatctacgaaatctgg	This paper	N/A
Primer *Chd5* reverse: gcatagccatgcgtcaca	This paper	N/A
Primer *Hand2* forward: ccgacaccaaactctccaa	This paper	N/A

Author Manuscript Author Manuscript Author Manuscript Author Manuscript

REAGENT or RESOURCE	SOURCE	IDENTIFIER
Primer *Hand2* reverse: gatccatgaggtaggcgatg	This paper	N/A
Primer *Phox2b* forward: ccgataaggaccacttttgg	This paper	N/A
Primer *Phox2b* reverse: tcggtgaagagtttgtatggaa	This paper	N/A
Primer *Sox10* forward: gacacggttttccacttcct	This paper	N/A
Primer *Sox10* reverse: ctcgtgaagagcccaacg	This paper	N/A
Primer *Th* forward: ctttgtgcgcttcgaggt	This paper	N/A
Primer *Th* reverse: cttgggaaccagggaacc	This paper	N/A
Software and Algorithms		
Prism 8	GraphPad Software	
R	Survival package	
Bowtie2	Langmead and Salzberg, 2012	http://bowtie-bio.sourceforge.net/bowtie2/index.shtml
ImageJ	Schneider et al., 2012	https://imagej.nih.gov/ij/